Increased adiposity in the retinol saturase-knockout mouse

Alexander R. Moise,*[,1] Glenn P. Lobo,* Bernadette Erokwu,[†,‡] David L. Wilson,[†,‡] David Peck,* Susana Alvarez,[§] Marta Domínguez,[§] Rosana Alvarez,[§] Chris A. Flask,[†,‡] Angel R. de Lera,[§] Johannes von Lintig,* and Krzysztof Palczewski*

*Department of Pharmacology, Case School of Medicine, [†]Department of Radiology, and [‡]Department of Biomedical Engineering, Case Western Reserve University, Cleveland, Ohio, USA; and [§]Departamento de Química Orgánica, Facultad de Química, Universidade de Vigo, Vigo, Spain

ABSTRACT **The enzyme retinol saturase (RetSat) catalyzes the saturation of all-*trans*-retinol to produce (*R*)-all-*trans*-13,14-dihydroretinol. As a peroxisome proliferator-activated receptor (PPAR) γ target, RetSat was shown to be required for adipocyte differentiation in the 3T3-L1 cell culture model. To understand the mechanism involved in this putative proadipogenic effect of RetSat, we studied the consequences of ablating RetSat expression on retinoid metabolism and adipose tissue differentiation in RetSat-null mice. Here, we report that RetSat-null mice have normal levels of retinol and retinyl palmitate in liver, serum, and adipose tissue, but, in contrast to wild-type mice, are deficient in the production of all-*trans*-13,14-dihydroretinol from dietary vitamin A. Despite accumulating more fat, RetSat-null mice maintained on either low-fat or high-fat diets gain weight and have similar rates of food intake as age- and gender-matched wild-type control littermates. This increased adiposity of RetSat-null mice is associated with up-regulation of PPARγ, a key transcriptional regulator of adipogenesis, and also its downstream target, fatty acid-binding protein 4 (FABP4/aP2). On the basis of these results, we propose that dihydroretinoids produced by RetSat control physiological processes that influence PPARγ activity and regulate lipid accumulation in mice.—Moise, A. R., Lobo, G. P., Erokwu, B., Wilson, D. L., Peck, D., Alvarez, S., Domínguez, M., Alvarez, R., Flask, C. A., de Lera, A. R., von Lintig, J., Palczewski, K. Increased adiposity in the retinol saturase-knockout mouse. *FASEB J.* 24, 1261–1270 (2010). www.fasebj.org**

Key Words: retinoic acid · dihydroretinol · retinol-binding proteins · retinoic acid receptor

VITAMIN A, ALL-*TRANS*-RETINOL (atROL), plays an essential role in the development and function of virtually all tissues. A well-regulated oxidation pathway converts dietary atROL to bioactive metabolites such as all-*trans*-retinoic acid (atRA) and 9-*cis*-retinoic acid, which regulate the expression of specific subsets of genes within target tissues *via* the ligand-activated transcription factors, retinoic acid receptors (RARs) and retinoid X receptors (RXRs), respectively (1–4). Several lines of evidence support a role for vitamin A metabolites in the regulation of fat reserves, adipocyte differentiation, and function (5, 6). Many of these effects are likely mediated *via* RARs, which, among other processes, control adipocyte differentiation (7–10), fat deposition (5, 11), oxidative metabolism in adipocytes (12), leptin expression (13, 14), and gluconeogenesis through the rate-limiting gluconeogenic enzyme phosphoenolpyruvate carboxykinase (15). There is a report that other retinoids, such as the atRA precursor retinaldehyde, also participate in the regulation of energy balance independently of atRA (16).

In vivo studies have demonstrated that vitamin A supplementation delays the onset of obesity in predisposed rats (17, 18). Administration of atRA was shown to repress obesity, increase insulin sensitivity, remodel white adipose tissue, and increase the rate of lipid oxidation in the skeletal muscle of mice (11, 19, 20). These studies are particularly relevant as adipose tissue is one of the most important tissues involved in the regulation of energy balance by storing energy in the form of fat and by acting as an endocrine organ that secretes hormones and cytokines (adipokines) (21, 22). Adipose tissue also acts as a storage depot for several essential lipid-soluble factors and vitamins. In addition to provitamin A carotenoids, it is estimated that 10–20% of the body's vitamin A content is stored as retinyl esters (REs) in adipocytes (23). Therefore, conversion of adipose stores of vitamin A to bioactive metabolites influences adipose tissue formation and function and plays a role in the prevention/therapy of obesity and other metabolic disorders.

We originally identified and characterized the enzyme retinol saturase (RetSat), which catalyzes the saturation of atROL to produce (*R*)-all-*trans*-13,14-dihydroretinol (DROL) (24–26). (*R*)-DROL undergoes oxidation by short- and medium-chain alcohol dehydrogenases and retinaldehyde dehydrogenases, leading to

[1] Correspondence: Department of Pharmacology and Toxicology, University of Kansas, Lawrence, KS, USA. E-mail: alexmoise@ku.edu

doi: 10.1096/fj.09-147207

formation of (*R*)-all-*trans*-13,14-dihydroretinoic acid (DRA), a potential ligand for RAR (26–28). Similar to atRA, levels of DRA are controlled *in vivo* in both a temporal and spatial manner through enzymes and transport factors involved in its synthesis and breakdown (27).

Recently, an association was proposed between RetSat and adipocyte differentiation and the responses mediated by PPARγ, a key transcriptional regulator of adipocyte differentiation (29). RetSat is expressed in most adult tissues but predominantly in liver, kidney, intestine, and adipose tissue. Expression of RetSat in adipose tissue is regulated by PPARγ through a PPAR response element (PPRE) present in the first intron of RetSat (30). As a consequence, the expression of RetSat is markedly induced during adipocyte differentiation (30). RetSat is a fibrate/thiazolidinedione-sensitive gene, suggesting that its product could be involved in insulin sensitivity. Indeed, RetSat expression is suppressed in insulin-resistant states, as noted in obese patients and genetically obese (*ob/ob*) mice (30). RetSat expression was also shown by some studies to be up-regulated and in others suppressed by a high-fat diet (HFD) in response to mediators of inflammation (30–32). More important, ablation of RetSat expression by siRNA blocked adipocyte differentiation, while ectopic expression of enzymatically active RetSat enhanced PPARγ activity and adipocyte differentiation in a cell culture model (30). However, exogenous supplementation with the product of RetSat, DROL, did not promote adipocyte differentiation of 3T3-L1 cells following silencing of RetSat expression (30). In fact, treatment of these cells with (*R*)-DROL led to inhibition of adipogenesis through activation of RARs (26). Thus, the mechanism involved in the proadipogenic effect of RetSat and its physiological relevance remains to be fully explored.

Here, we studied the role of RetSat during adipocyte differentiation by examining adipocyte tissue development and function in mice that have inactivated RetSat by homologous recombination. For this, we established *RetSat*$^{-/-}$ mice as a mouse model deficient in (*R*)-DROL. Our studies indicate that *RetSat*$^{-/-}$ mice fed either low-fat diets (LFDs) or HFDs gain weight at a similar rate as their wild-type littermates and show normal insulin resistance and glucose tolerance. However, *RetSat*$^{-/-}$ mice exhibit increased adiposity and increased expression of key adipogenic markers while maintained on an HFD. These results suggest that RetSat-deficiency is associated with alterations in the *in vivo* adipogenic program leading to increased fat deposition; however, RetSat is not an essential requirement for adipocyte differentiation as previously proposed, on the basis of tissue culture model results (30).

MATERIALS AND METHODS

Chemical syntheses

Chemical syntheses of (*R*)-DROL was performed, and the enantiomeric purity of dihydroretinoids was verified by chiral high-performance liquid chromatography (HPLC), as described previously (26).

Targeting construct, electroporation of embryonic stem (ES) cells, and generation of *RetSat*$^{-/-}$ chimeras

To obtain homozygous *RetSat*$^{-/-}$ mice, we used homologous recombination in ES cells to replace exon 1 of the wild-type *RetSat* gene with a neomycin resistance expression cassette (*neoR*) (**Fig. 1*A***). Clones were isolated by PCR screening from a 129SvJ mouse bacterial artificial chromosome (BAC) library (Genome Systems, St. Louis, MO, USA). A 10.5-kbp region in the genomic sequence surrounding the 5′ end of the *RetSat* gene was used to construct the targeting vector. The region was designed such that the short homology arm extended 1.3 kbp 3′ to exon 1 and included exon 2, and part of exon 3. The long homology arm extended 7.2 kbp upstream of exon 1, while the short homology arm extended 1.3 kbp downstream of exon 1. The *neoR* cassette replaced ~2 kbp of the RetSat gene, including exon 1 containing the translation start ATG (Fig. 1*A*). The targeting vector was confirmed by restriction analysis and sequencing. The targeting vector was linear-

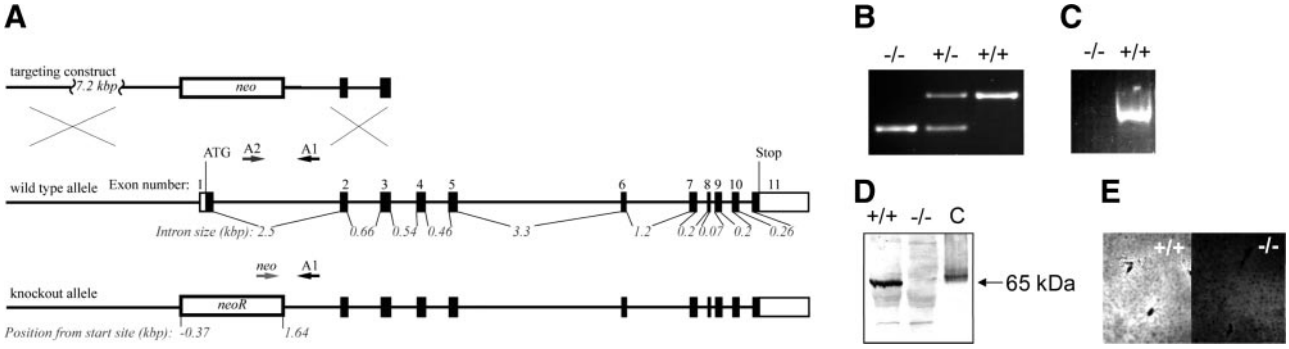

Figure 1. Generation of *RetSat*$^{-/-}$ mice by homologous recombination. *A*) Targeting vector was designed to replace exon 1 with a neomycin resistance cassette (*neoR*). *B*) Genotyping was performed by PCR with the primer pair A2 and A1 used for the wild-type allele and *neo* and A1 for the knockout allele. *C*) RT-PCR of RNA isolated from the liver of *RetSat*$^{-/-}$ and *RetSat*$^{+/+}$ mice using primers directed against exon 1 and exon 4 shows that there was no detectable message in *RetSat*$^{-/-}$ mice that includes this region. *D*) Immunoblotting of lysates of RetSat transfected cells or liver lysates from *RetSat* $^{-/-}$ and *RetSat*$^{+/+}$ mice indicates that RetSat protein is not expressed in *RetSat*$^{-/-}$ mice. *E*) Immunohistochemistry of liver sections from *RetSat*$^{-/-}$ and *RetSat*$^{+/+}$ also confirms the absence of RetSat protein in the liver of *RetSat*$^{-/-}$ mice.

ized with *Not*I and then transfected by electroporation into ES cells. After selection in neomycin-containing medium, G418-surviving colonies were expanded. PCR analysis was performed to identify ES clones that had undergone homologous recombination. Positive ES clones were identified by using primer pairs 5′-AAACTAGGGATGCTAATCATGGTG and 5′-TGCGAGGCCAGAGGCCACTTGTGTAGC with the expected PCR product of 1.63 kbp. Correctly targeted recombinant ES clones were microinjected into C57BL/6 blastocysts. Chimeric mice were generated and screened for germ line transmission of the disrupted *RetSat* gene. Chimerism was estimated according to the coat color of the litter. Male chimeric mice then were backcrossed with female C57BL/6 mice to produce heterozygous and subsequently homozygous *RetSat*$^{-/-}$ mice.

Genotyping *RetSat*$^{-/-}$ and *RetSat*$^{+/+}$ mice

To identify the wild-type allele, we used the primer pair A1 5′-TGAATGCAAGCGAGGAAAGA and A2 5′- CCATGGCTTGGATGGAGATT (670-bp PCR product). The knockout allele was identified with primer pair A1 5′-TGAATGCAAGCGAGGAAAGA and *neo* 5′-TGCGAGGCCAGAGGCCACTTGTGTAGC (434-bp PCR product). PCR conditions were 94°C for 30 s; 60°C for 30 s; and 72°C for 120 s for a total of 30 cycles.

Animal husbandry and diets

Because the *RetSat*$^{-/-}$ mouse strain was maintained through mating of heterozygous siblings from one generation to the next without backcrossing, the resulting progeny had a mixed genetic background (129sv/C57BL6). All animal experiments employed procedures approved by the Case Western Reserve University Animal Care Committee and conformed to recommendations of the American Veterinary Medical Association Panel on Euthanasia and recommendations of the Association of Research for Vision and Ophthalmology (ARVO). Mice were maintained under environmentally controlled conditions (24°C, 12:12-h light-dark cycle) with *ad libitum* access to food and water. During breeding and lactation periods, mice were maintained on an LFD based on the AIN92 formulation, containing 10 kcal % fat (D12450B) supplemented with 4 IU vitamin A/g diet and prepared by Research Diets (New Brunswick, NJ, USA). Two-month-old sex-matched male and female *RetSat*$^{-/-}$ and *RetSat*$^{+/+}$ mice were randomly distributed into 8 groups (n=6/group). During the 12-wk experimental period, these mice were fed *ad libitum* either the LFD or an HFD containing 45 kcal % fat (D12451) and 4 IU vitamin A/g diet (Research Diets). Body weight was determined twice a week over the total experimental period. Food intake was estimated on a per-cage basis from the actual amount of food consumed and its caloric equivalence. At the end of the treatment period, the mice were sacrificed by CO_2 inhalation between 9:30 and 11:30 AM. All animal experiments were conducted in accordance with the National Institutes of Health (NIH) Guide for the Care and Use of Laboratory Animals.

RNA preparation and quantitative real-time PCR (qRT-PCR)

RNA was extracted from mouse adipose tissue with the TRIzol reagent (Invitrogen, Carlsbad, CA, USA) and purified by using the RNeasy system (Qiagen, Valencia, CA, USA). Approximately 2 μg of total RNA was reverse-transcribed with the High Capacity RNA-to-cDNA kit (Applied Biosystems, Foster City, CA, USA) following the manufacturer's instructions. Quantitative PCR (qPCR) was carried out by using TaqMan chemistry, with TaqMan Gene Expression Master Mix and Assays on Demand probes (Applied Biosystems) for mouse PPARγ (Mm01184323_m1) and mouse Fabp4/aP2 (Mm00445880_m1), respectively. 18s rRNA (4319413E) (Applied Biosystems) was used as the endogenous control. All real-time experiments were performed in triplicate with the Applied Biosystems Step-One Plus qRT-PCR machine. Gene expression analysis was quantified according to the manufacturer's protocol, and data are presented as fold changes.

Immunoblot analyses

For determination of RetSat protein levels, we used the previously described anti-RetSat monoclonal antibody at a dilution of 1:1,000. For the Ras-related nuclear protein (RAN) protein loading control, the antiserum AB6046 (Abcam, Cambridge, UK) was used at a dilution of 1:500. Secondary antibodies were alkaline phosphatase-conjugated anti-rabbit and anti-mouse IgG whole molecules (Sigma, St. Louis, MO, USA). Immunoblots were developed with a colorimetric detection system (Sigma).

Determinations of tissue and serum lipids and glucose and insulin tolerance tests (GTTs and ITTs)

Determinations of nonesterified free fatty acids (NEFAs), triglycerides (TGs), cholesterol, and phospholipids in liver tissues of *RetSat*$^{-/-}$ and *RetSat*$^{+/+}$ mice were carried out by the Mouse Metabolic Phenotyping Center (University of Cincinnati, Cincinnati, OH, USA). GTTs were performed using *RetSat*$^{-/-}$ and *RetSat*$^{+/-}$ male littermates (derived from *RetSat*$^{-/-}$ and *RetSat*$^{+/-}$ crossings) by intraperitoneal (i.p.) injection of dextrose (1 or 2 g/kg body weight) after overnight food deprivation. Mice were weighed, and venous blood for the fasting glucose level (at time 0) was drawn from a small incision in the tail. Glucose suspended in sterile PBS (20% w/v) was injected i.p., according to weight. Blood was collected from the tail vein at 30, 60, 90, and 120 min after injection, and plasma glucose was measured by using a glucometer (Accu-Chek Aviva; Roche Applied Science, Indianapolis, IN, USA). ITTs were performed after 4 h food deprivation. The protocol then followed that of the GTT, with the exceptions that mice were injected i.p. with insulin (humalin 100 U/ml) to obtain 0.8 U/kg of body weight, and blood was collected at 15, 30, 60, and 90 min after injection. Results of both the GTTs and ITTs were analyzed by 1-way ANOVA. Area under the curve (AUC) analyses were independent of baseline glucose values.

Histology and immunohistochemistry

For paraffin sections, livers were fixed in neutral buffered formalin and processed into paraffin blocks. Representative histological sections of each specimen were stained with hematoxylin/eosin (Merck, Whitehouse Station, NJ, USA) according to a described standard staining method (33). For immunohistochemistry, liver sections were fixed in 4% paraformadehyde overnight and then cryoprotected in 30% sucrose for a second night, following which the liver samples were embedded in Tissue-Tek O.C.T. compound (Sakura Finetechnical, Tokyo, Japan) and cut into 8-μm-thick slices. Sections were stained with anti-RetSat rabbit polyclonal antibody at 1:100 dilution and then Alexa 488-conjugated goat anti-rabbit secondary antibody at 1:1000 dilution. Sections were analyzed under a Leica fluorescent microscope (Leica Microsystems, Deerfield, IL, USA), and images were captured with a digital camera.

Estimation of body composition and adiposity by MRI

Body composition and percentage adiposity were assessed with iterative decomposition with echo asymmetry and least-squares estimation (IDEAL) magnetic resonance imaging (MRI) techniques (34). The IDEAL MRI images were post-processed offline by using a previously described methodology to correct for receive-field inhomogeneities and magnetic relaxation (35). Each mouse was positioned at the isocenter of a Bruker Biospec 7T MRI scanner (Bruker Corp., Billerica, MA, USA). Mice were provided with isoflurane anesthesia continuously during the imaging procedures *via* a nose cone. Animals' respiration rates and core body temperatures were maintained at 30–60 breaths/min and 35 ± 1°C. Coronal, high-resolution (1 mm × 200 μm × 200 μm) multiple-spin echo acquisition with respiratory gating was used to acquire MRI images of the entire animal. This acquisition was repeated with different echo shifts as typical for IDEAL acquisitions to obtain the final fat ratio images that were used to robustly segment the lipid (visceral and subcutaneous) from the water/tissue compartments (35). The segmentation results for each imaging slice were compiled to measure the total subcutaneous and total visceral adipose tissue.

Retinoid analyses

All experimental procedures related to extraction, derivatization, and separation of retinoids were carried out under dim red light (27). The organic extraction protocol used was a modification of the mass spectrometry (MS)-compatible reverse-phase liquid chromatography (LC) method of Kane *et al.* (36, 37), as described by Moise et al. (27). HPLC or tandem LC-MS/MS was used to identify retinoids and dihydroretinoid metabolites. Only glass containers, pipettes, and calibrated syringes were employed during retinoid extraction. Serum, visceral fat, and liver tissues from *RetSat*$^{-/-}$ and *RetSat*$^{+/+}$ mice were homogenized in 137 mM NaCl, 2.7 mM KCl, and 10 mM sodium phosphate (pH 7.4) for 30 s with a Polytron homogenizer. Polar retinoids were deprotonated by adding NaOH to 1 ml of each ethanolic extract (NaOH, 75 mM final concentration), and nonpolar retinoids were extracted with 5 ml of hexane. The extraction was repeated once, and the combined organic phases were dried under vacuum, resuspended in hexane, and examined by normal-phase HPLC with a Beckman Ultrasphere Si 5-μm, 4.6- × 250-mm column (Beckman Coulter, Fullerton, CA, USA). Elution was carried out with an isocratic solvent system consisting of 10% ethyl acetate in hexane (v/v) for 25 min at a flow rate of 1.4 ml/min at 20°C with ultraviolet (UV) detection at 325 and 290 nm for nonpolar retinoids and dihydroretinoids, respectively. Nonpolar retinoids were identified by comparing their spectra and elution times with those of authentic standards. The fraction corresponding to DROL was collected, dried, and repurified by normal-phase HPLC. The repurified fraction was then dried, resuspended in hexane, and examined by chiral HPLC, as described previously (26). The (*R*) and (*S*) enantiomers of DROL were separated by chiral HPLC by using a chiral HPLC column (Chiralcel OD cellulose column; Daicel Chemical Industries, Osaka, Japan; 10 μm, 250×4.6 mm), and a mobile phase of 1.0% isopropanol in hexane, at a flow rate of 1.0 ml/min, 20°C. Confirmation of the analytes was done by LC-MS/MS with a Thermo Scientific LXQ Linear Ion Trap Mass Spectrometer (Thermo, Waltham, MA, USA) equipped with atmospheric pressure chemical ionization (APCI) in a positive-ion mode. atROL (*m/z* 269, $[M\text{-}H_2O+H]^+$), and DROL (*m/z* 289 $[M+H]^+$) were monitored in the selected ion monitoring (SIM) mode.

Statistical analyses

Data are presented as means ± SD. The Student's *t* test was used to analyze data between the controls and knockout strains, with values of $P \leq 0.05$ considered to be statistically significant.

RESULTS

Establishing *RetSat*$^{-/-}$ and dihydroretinoid-deficient mice

To investigate the physiological consequences of RetSat ablation, we disrupted exon 1 of the murine *RetSat* gene by homologous recombination, thereby eliminating the ATG start codon, the promoter, and the putative PPRE present in intron 1 (Fig. 1*A*). Mice were genotyped by using primers directed against the right junction of the *neoR* expression cassette (Fig. 1*B*). We verified that the expression of RetSat was abolished by RT-PCR with primers directed against exon 1 and exon 4 (Fig. 1*C*). No transcripts that included this region were detected in livers of *RetSat*$^{-/-}$ mice. We then studied the expression of RetSat protein by using both SDS-PAGE and immunoblotting of liver lysates and immunohistochemistry of liver sections from *RetSat*$^{-/-}$ mice. Both assays revealed the absence of any immunoreactive RetSat polypeptide in livers of these animals (Fig. 1*D, E*). The epitope used to raise the anti-RetSat monoclonal antibody and polyclonal antiserum was a histidine-tagged fragment encoding the ^{148}MASPF. . . MTALVPM^{465} of RetSat polypeptide encompassing a region encoded by exons 3 to 9. For this reason the antibodies recognized a region much larger than that disrupted in exon 1. This experiment provides evidence for absence of truncated polypeptide products being expressed from the *RetSat* gene that might be generated from an internal start site downstream of exon 1.

We next evaluated the formation of (*R*)-DROL in *RetSat*$^{-/-}$ mice gavaged with retinyl palmitate. Mouse RetSat and its orthologues from zebrafish and humans are currently the only enzymes known to catalyze the saturation of ROL to (*R*)-DROL. Therefore, it was important to determine whether there are other enzymes that could compensate for this activity in *RetSat*$^{-/-}$ mice. Because RetSat is the most highly expressed in the liver (25, 30), we chose this tissue to assess levels of DROL in *RetSat*$^{-/-}$ mice. Mice were gavaged with retinyl palmitate, and their hepatic nonpolar retinoids were analyzed for the presence of (*R*)-DROL by HPLC coupled to UV detection, as described previously (27). Using this method, we identified a peak corresponding to DROL in *RetSat*$^{+/+}$ mice, but not in *RetSat*$^{-/-}$ mice (**Fig. 2**). To improve detection of very low levels of dihydroretinoids, we developed a specific method based on chiral HPLC coupled with MS to analyze the purified fraction corresponding to DROL obtained by normal-phase HPLC chromatography of the organic extract of livers of *RetSat*$^{+/+}$ mice. Then, we also collected the corresponding fraction of

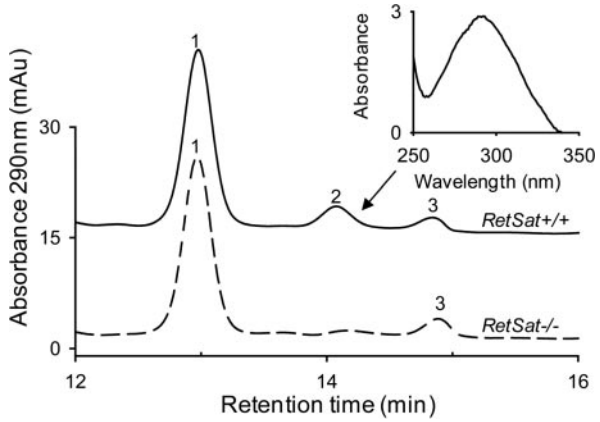

Figure 2. Analysis of nonpolar retinoids extracted from the livers of *RetSat*$^{-/-}$ and *RetSat*$^{+/+}$ mice. *RetSat*$^{-/-}$ and *RetSat*$^{+/+}$ mice were gavaged with retinyl palmitate. Two hours post-treatment, livers were dissected, and retinoids were saponified, organically extracted, and examined by normal-phase HPLC. Extractions were normalized to the amount of tissue used. Retinoids were identified on the basis of their online UV-visual absorbance spectra and by their elution profiles compared with authentic standards. Peaks identified were peaks 1 (13-cis-retinol), 2 (DROL), and 3 (9,13-di-*cis*-retinol); other retinoid peaks eluting outside the 12- to 16-min range were omitted for clarity. The *RetSat*$^{-/-}$ mouse chromatogram (dashed line) shows that DROL was not detected in *RetSat*$^{-/-}$ mice gavaged with retinyl palmitate. Inset shows the UV-visual spectrum of DROL isolated from livers of *RetSat*$^{+/+}$ mice.

the organic extract of livers obtained from *RetSat*$^{-/-}$ mice eluted during the same time interval as DROL (13–15 min postinjection). Both fractions were dried and reanalyzed on a chiral HPLC system described previously (21) that was coupled to an MS/MS detector. To increase sensitivity, SIM was used to detect an ion species corresponding to (*R*)-DROL (*m/z* 289 $[M+H]^+$). Chiral HPLC analysis has the advantage of being able to distinguish (*R*)-DROL generated by RetSat from its enantiomer (*S*)-DROL. On the basis of this analysis, we could reliably detect DROL in the livers of retinyl palmitate-supplemented *RetSat*$^{+/+}$ but not *RetSat*$^{-/-}$ mice. Chiral HPLC-MS/MS analysis of the organic extracts of *RetSat*$^{+/+}$ mouse liver indicated that DROL is predominantly present as the (*R*)-DROL enantiomer *in vivo* (Supplemental Fig. 1), as noted previously (26). A smaller peak corresponding to (*S*)-DROL was also identified in *RetSat*$^{+/+}$ mouse liver based on its chromatographic properties, UV-visual spectrum, mass, and fragmentation spectra compared to authentic standards (Supplemental Fig. 1). Given that (*S*)-DROL could not be detected in the liver of *RetSat*$^{-/-}$ mice and that RetSat is known to produce exclusively (*R*)-DROL (26), this finding suggests that (*S*)-DROL is likely a partial racemization product of (*R*)-DROL. We were not able to assess the levels of dihydroretinoids in the adipose tissue of *RetSat*$^{-/-}$ and *RetSat*$^{+/+}$ mice because levels of DROL in adipose tissue were below the detection limits of our instrument. On the basis of the analysis of the hepatic levels of DROL, we conclude that *RetSat*$^{-/-}$ mice cannot convert atROL to (*R*)-DROL, and thus are deficient in dihydroretinoid production.

Assessment of retinoids and hepatic lipid levels in *RetSat*$^{-/-}$ mice

Because RetSat was described as a retinoid-processing enzyme, it is important to determine whether conversion of atROL to (*R*)-DROL *in vivo* leads to alterations in endogenous retinoid levels. To establish whether RetSat-deficiency has a global effect on retinoid levels, we analyzed retinoid levels in liver, serum, and adipose tissue of *RetSat*$^{-/-}$ and *RetSat*$^{+/+}$ mice. For this experiment, male and female *RetSat*$^{-/-}$ mice and *RetSat*$^{+/+}$ littermates were maintained on a vitamin A-sufficient LFD containing 4 IU/g diet and 10 kcal % fat. We then analyzed retinol and retinyl ester levels in the liver, adipose tissues, as well as levels of retinol circulating in serum. To extract retinoids from adipose tissue efficiently, the extract had to be saponified to convert retinyl esters to retinol. So by measuring retinol levels following saponification, we actually measured total levels of retinoids in adipose tissue. Livers of both male and female *RetSat*$^{-/-}$ and *RetSat*$^{+/+}$ mice contained similar levels of retinyl esters (**Fig. 3**). Levels of free retinol in liver and serum did not differ significantly between these genotypes, but such levels were generally higher in males than females (Fig. 3). There were no significant differences in total retinoid levels in fatty tissues of *RetSat*$^{-/-}$ and *RetSat*$^{+/+}$ mice (Fig. 3). Low levels of retinaldehyde and retinoic acid were detect-

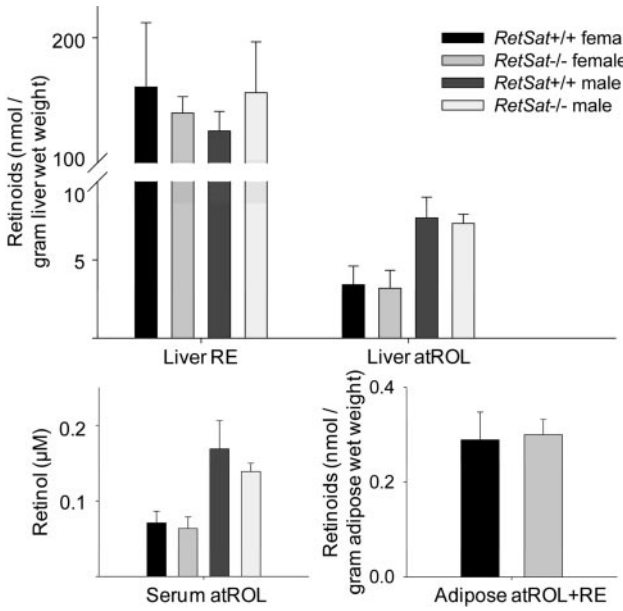

Figure 3. Levels of nonpolar retinoids in tissues of *RetSat*$^{-/-}$ and *RetSat*$^{+/+}$ mice. All-*trans*-retinol (atROL) and retinyl esters (RE) extracted from liver, serum and visceral adipose tissues of *RetSat*$^{-/-}$ and *RetSat*$^{+/+}$ mice were examined by normal-phase HPLC. Amounts loaded were normalized on the basis of the amount of tissue. Levels of retinoids were quantified on the basis of their absorbance over time (AUC) compared to that of known amounts of standards.

able in the livers of both genotypes, but the amounts of these compounds were too close to the detection limit of the instrument to allow accurate quantification. Therefore, our estimate of levels of major retinoids, such as retinol and retinyl esters, indicates that these are not significantly altered in *RetSat*$^{-/-}$, as compared to *RetSat*$^{+/+}$ mice.

We next assayed hepatic levels of TGs, cholesterol, phospholipids, and NEFA in male and female *RetSat*$^{-/-}$ and *RetSat*$^{+/+}$ mice maintained on a normal *ad libitum* diet. These assays indicate that there were no significant genotypic differences in the levels of TGs, cholesterol, phospholipids or NEFAs between *RetSat*$^{-/-}$ and *RetSat*$^{+/+}$ animals (**Fig. 4**), even though males and females of either genotype showed gender-specific differences in the levels of these metabolites. These results indicate that there were no alterations in the levels of hepatic lipids as a result of RetSat-deficiency in *RetSat*$^{-/-}$ mice.

Assessment of growth curves, adiposity, and glucose homeostasis in *RetSat*$^{-/-}$ mice

Previous studies suggest that expression of RetSat is up-regulated and mandatory for adipocyte differentiation in a cell culture model. We used the 3T3-L1 cell culture model of adipocyte differentiation to study induction of RetSat during adipocyte differentiation. 3T3-L1 cells were induced to differentiate according to a standard protocol that employed a hormonal cocktail composed of 3-isobutyl-1-methylxanthine (IBMX), dexamethasone, and insulin (IDI). The expression of RetSat was studied by immunoblotting the resulting cell lysates. Expression of RetSat protein was noticeably increased 2 d after addition of this cocktail (d 4 in Supplemental Fig. 2), and maintained at high levels during the insulin-only and mature adipocyte stages (d 6 and 9 in Supplemental Fig. 2). This timeframe of induction is consistent with previous

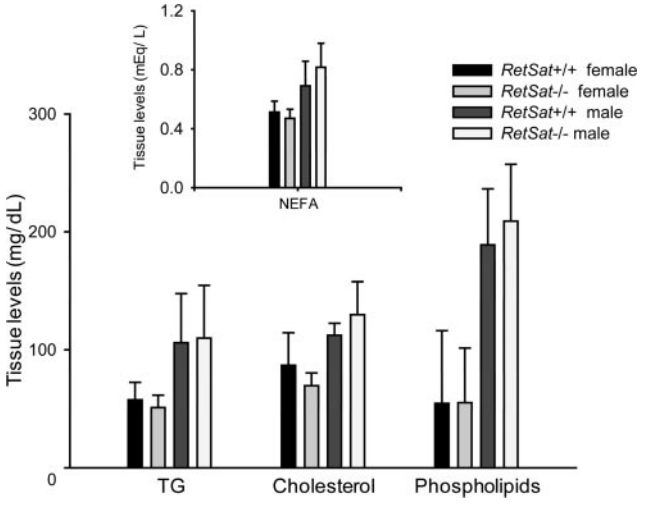

Figure 4. Hepatic lipid levels of 12-wk-old male and female *RetSat*$^{-/-}$ and *RetSat*$^{+/+}$ mice maintained on normal chow. TGs, cholesterol, phospholipids, and NEFAs were assayed in the fed state.

results (30). Our results, therefore, confirm that expression of RetSat protein is up-regulated during adipocyte differentiation and suggest a role for this enzyme during adipocyte differentiation and in mature adipocytes in cell culture.

To learn whether RetSat plays a role in adipocyte differentiation *in vivo,* we determined weight gain and adiposity in *RetSat*$^{-/-}$ mice and their *RetSat*$^{+/+}$ littermates maintained on diets of varied fat content. Male and female *RetSat*$^{-/-}$ and *RetSat*$^{+/+}$ mice initially were maintained on an LFD containing 10 kcal % fat for 2 mo. At 2 mo of age, we then provided these mice with either the control LFD (10 kcal % fat) or an HFD containing 45 kcal % fat. Food intake and body weight were monitored twice a week. *RetSat*$^{-/-}$ mice did not show significant differences in weight gain compared to *RetSat*$^{+/+}$ controls when maintained on either the low- or high-fat diet (**Fig. 5**). This finding argues that the block in adipocyte differentiation following ablation of RetSat does not result in alterations in total body weight gain but could still affect the relative composition and size of adipose stores.

Therefore, we next used MRI to image adiposity in *RetSat*$^{-/-}$ mice and *RetSat*$^{+/+}$ littermates maintained on an HFD. During their breeding and lactation periods, these mice were maintained on an LFD. Then 2-mo-old sex-matched female *RetSat*$^{-/-}$ mice and *RetSat*$^{+/+}$ littermates were randomly distributed into 4 groups. During the experimental period, mice were fed an HFD (45 kcal % fat) for 10 wk, after which we determined their body composition and calculated an adiposity index by using MRI. MRI is a technique uniquely capable of acquiring data to estimate adipose volumes in various regions and in all major organs and tissues, as well as in visceral adipose tissue. These analyses revealed that both male and female *RetSat*$^{-/-}$ mice contained a larger percentage of adipose tissue stores than their *RetSat*$^{+/+}$ counterparts despite having comparable body weights and similar food intakes (**Fig. 6*A***). The increased adiposity manifested in *RetSat*$^{-/-}$ mice was a general increase in the volume of visceral and inguinal adipose stores, as revealed by MRI analyses (Fig. 6*B*). Histology of adipose stores showed that adipocytes in *RetSat*$^{-/-}$ mice had a normal morphology and therefore did not show impaired adipocyte differentiation (**Fig. 7**). Though there were some variations in the size of the adipose cells and the degree of macrophage infiltration in tissues obtained from different animals, these differences were not statistically significant and were not consistently observed when comparing *RetSat*$^{-/-}$ and *RetSat*$^{+/+}$ mice. Interestingly, the histology of liver tissue from *RetSat*$^{-/-}$ mice and *RetSat*$^{+/+}$ littermates maintained on a HFD failed to show increased accumulation of lipids, indicating that the increased adiposity was not associated with a fatty liver phenotype during the 10-wk period of HFD treatment (Fig. 7).

We then determined whether *RetSat*$^{-/-}$ mice develop insulin resistance or impaired glucose tolerance. Male *RetSat*$^{-/-}$ and *RetSat*$^{+/-}$ mice were initially maintained on normal chow. At 3 mo of age, we examined

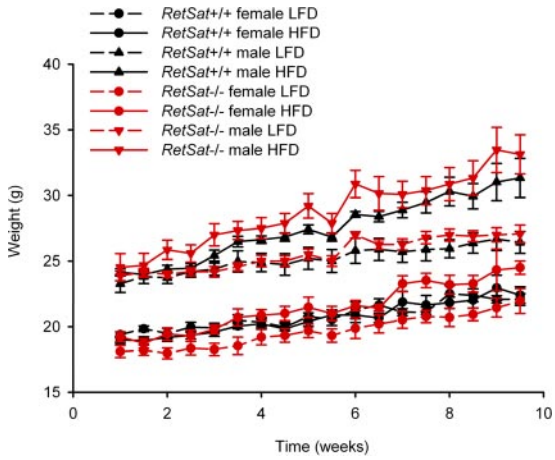

Figure 5. Growth curves of male and female *RetSat*$^{-/-}$ and *RetSat*$^{+/+}$ mice maintained on either an LFD containing 10 kcal % fat or an HFD containing 45 kcal % fat. Groups of 6 male or female *RetSat*$^{-/-}$ or *RetSat*$^{+/+}$ mice were maintained on normal chow until 2 mo of age, then treated with either an LFD or HFD for 10 wk. Food intake and body weight were monitored 2×/wk. *RetSat*$^{-/-}$ mice did not show statistically significant differences from wild-type controls fed either diet in terms of weight gain or food intake (not shown). Values are presented as means ± SD.

plasma glucose levels after an intraperitoneal glucose load (GTT) or an injection of insulin (ITT). Our results showed a statistically significant ($P \leq 0.05$) increase in glucose levels in both male and female *RetSat*$^{-/-}$ compared with *RetSat*$^{+/-}$ mice at 15 and 30 min after a glucose load (Supplemental Fig. 3). However, the overall response to this GTT did not differ between *RetSat*$^{-/-}$ and *RetSat*$^{+/-}$ mice, as deduced by analyzing AUCs of the respective plasma glucose curves. Glucose levels also were similar between *RetSat*$^{-/-}$ and *RetSat*$^{+/-}$ mice during the ITT (Supplemental Fig. 3), indicating that RetSat-deficiency does not result in insulin resistance or induce a diabetic phenotype in *RetSat*$^{-/-}$ mice maintained on a normal diet.

These results suggest that RetSat plays a role in adipocyte physiology and that RetSat-deficiency *in vivo* leads to enhanced adiposity in *RetSat*$^{-/-}$ mice. These observations are contrary to previous cell culture studies, indicating a requirement for RetSat for adipocyte differentiation.

RetSat deficiency leads to up-regulation of PPARγ and PPARγ target expression

Given the increased adiposity of *RetSat*$^{-/-}$ mice, we evaluated mRNA expression of PPARγ, a master regulator of adipocyte development and function, along with one of its best characterized targets, adipocyte protein 2 (aP2), in the adipose tissues of *RetSat*$^{-/-}$ and *RetSat*$^{+/+}$ mice maintained on an HFD (45 kcal % fat). Our results indicate that both PPARγ and its target aP2 were up-regulated in *RetSat*$^{-/-}$ mice compared with their *RetSat*$^{+/+}$ counterparts (**Fig. 8**). These findings support those of increased adiposity in *RetSat*$^{-/-}$ mice and argue that RetSat deficiency leads to increased fat deposition through up-regulation of factors that control the adipogenic program.

DISCUSSION

RetSat$^{-/-}$ mice are dihydroretinoid deficient and display increased adiposity

RetSat and homologues of RetSat have been identified in most animal species examined and all assayed enzymes (encoded by human, mouse, zebrafish, and starlet sea anemone genomes) display a high degree of sequence conservation and evidence the same activity profile by catalyzing the saturation of atROL double bonds to produce dihydroretinoids. These observations support a role for RetSat in vitamin A metabolism.

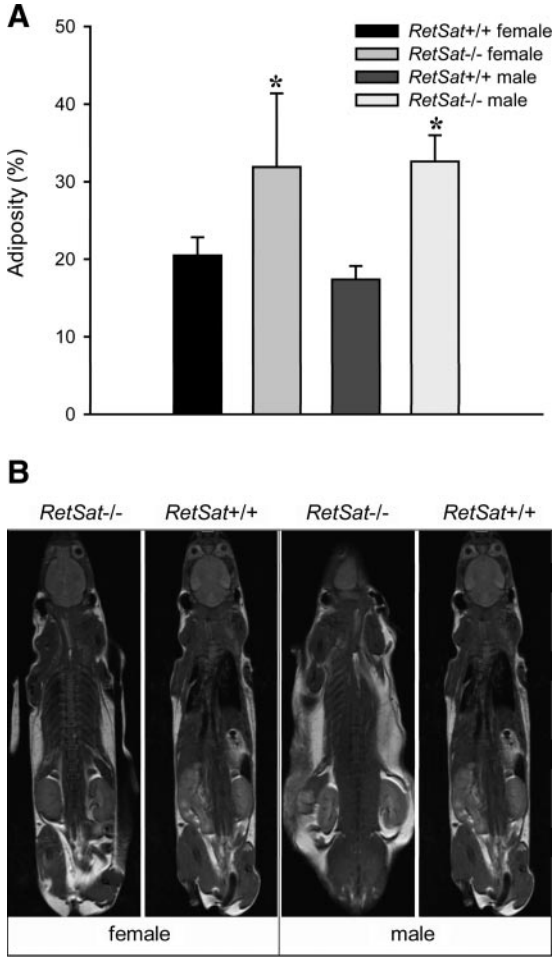

Figure 6. Adiposity in male and female *RetSat*$^{-/-}$ and *RetSat*$^{+/+}$ mice maintained on an HFD containing 45 kcal % fat. Male and female *RetSat*$^{-/-}$ or *RetSat*$^{+/+}$ mice (3/group) were maintained on normal chow until 2 mo of age, then treated with an HFD for 10 wk. *A*) At the end of treatment, adiposity was assessed by MRI and expressed as a percentage of total body weight. *B*) Representative MRI scans showing fat-only volumes reveal increased adipose tissue accumulation in female *RetSat*$^{-/-}$ mice maintained on the HFD. Values represent means ± SD; $n = 3$ animals/genotype. *$P < 0.05$.

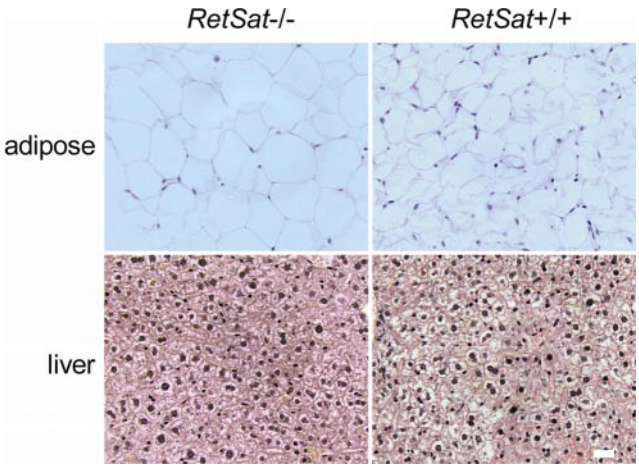

Figure 7. Normal liver and adipose tissue morphology and absence of liver lipid accumulation in *RetSat*$^{-/-}$ and *RetSat*$^{+/+}$ mice maintained on the HFD. Slides show representative histological sections of epididymal adipose tissue (top panels) and liver (bottom panels) from *RetSat*$^{-/-}$ and *RetSat*$^{+/+}$ mice maintained on the HFD for 10 wk. Tissues were stained with hematoxylin and eosin.

Results derived from ablation of RetSat expression in a tissue culture model of adipogenesis suggest that RetSat also is mandatory for adipocyte differentiation *in vitro* (30). Our results confirm that, as a direct PPARγ target, RetSat protein expression is dramatically induced during adipocyte differentiation in cell culture. To determine the role of RetSat in both vitamin A metabolism and adipose tissue physiology *in viv*o, we engineered a RetSat-deficient mouse model (Fig. 1). Our studies show that RetSat is indeed required for the formation of (*R*)-DROL *in vivo* and that there are no other enzymes that can compensate for its lack in *RetSat*$^{-/-}$ mice. However, the absence of dihydroretinoid production did not lead to global changes in the levels of nonpolar retinoids in the adipose tissue, plasma, or liver of *RetSat*$^{-/-}$ mice. Contrary to expectations from the *in vitro* studies (30), we found that RetSat deficiency did not lead to impaired adipose tissue formation *in vivo*. In fact, our results demonstrate that *RetSat*$^{-/-}$ mice have increased adiposity and increased expression of PPARγ and a PPARγ target, namely aP2. Moreover, adipocytes of *RetSat*$^{-/-}$ mice displayed normal morphology and *RetSat*$^{-/-}$ mice on either a high- or low-fat diet gained weight at rates comparable to their *RetSat*$^{+/+}$ littermates. *RetSat*$^{-/-}$ and *RetSat*$^{+/+}$ mice also showed similar levels of hepatic lipids, normal hypoglycemic responses to insulin, and comparable levels of plasma glucose following an intraperitoneal glucose challenge. Increased expression of PPARγ and PPARγ targets might allow *RetSat*$^{-/-}$ mice to maintain normal insulin sensitivity and glucose responses despite increased fat accumulation. This response may mimic the effect of synthetic PPARγ ligands, such as thiazolidinedones (TZDs), which activate PPARγ and induce adipogenesis while improving sensitivity to insulin. The increased adiposity and enhanced expression of PPARγ observed in *RetSat*$^{-/-}$ mice argues that RetSat plays a role in adipocyte biology, but it does not promote adipogenesis and is not required for adipocyte differentiation *in vivo*.

Dihydroretinoids contribute to the regulation of adipose tissue function by vitamin A

Both vitamin A-deficient mice (38) and mice deficient in classic retinoid pathway enzymes, such as retinol dehydrogenase 1 (39), retinaldehyde dehydrogenase (16), and retinyl ester hydrolase/hormone-sensitive lipase (40), show evidence of altered adiposity as a consequence of global disruption of retinoid levels. These effects were attributed to alterations in the levels of known retinoid metabolites, such as retinadehyde or retinoic acid. Because the absence of RetSat had no effect on the global levels of retinoids, our results suggest that low abundance but otherwise highly potent vitamin A metabolites could regulate pathways involved in neutral lipid accumulation.

The increased adiposity caused by RetSat deficiency resembles the phenotype observed in other mouse models deficient in retinoid-processing enzymes such as the retinol dehydrogenase 1 (RDH1)-deficient mouse (39) and mice deficient in carotenoid-15,15′-oxygenase (CMO1) (41). Moreover, dietary-induced vitamin A deficiency has been shown to cause a marked increase in adiposity, hypertrophy of white adipose tissue depots, and enhanced expression of PPARγ (38). But in contrast to vitamin A-deficient mice or knockout mouse models, such as RDH1, *RetSat*$^{-/-}$ mice lacking dihydroretinoids did not show alterations in the levels of other retinoids. So lack of RetSat *in vivo* only affects downstream metabolites, dihydroretinoids, without influencing global vitamin A status. The increased adiposity observed in *RetSat*$^{-/-}$ mice might result from a lack of dihydroretinoids, and thus caused by a different mechanism than the one currently proposed to explain the

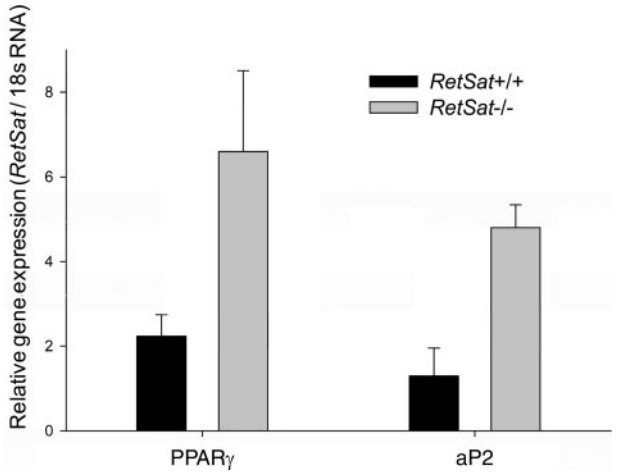

Figure 8. Adipose tissues from *RetSat*$^{-/-}$ mice show elevated PPARγ and aP2 mRNA expression. Relative adipose mRNA levels of PPARγ (*A*) and aP2 (*B*), as determined by qRT-PCR normalized to 18s rRNA. Values represent means ± SD; $n = 3$ animals/genotype. $^*P \leq 0.001$.

phenotype of vitamin A-deficient or RDH1-deficient mice.

Role of RetSat during adipocyte differentiation

While more studies are needed to establish the role of RetSat during adipocyte differentiation *in vivo*, it is already clear that the effect of RetSat on adipogenesis in the 3T3-L1 preadipocyte cell line does not mimic the *in vivo* situation in which ablation of RetSat leads to increased adiposity. This contradiction reflects the complexity of adipocyte differentiation process and the multitude of signaling cascades involved in this process. Indeed, certain signaling molecules and gene products have divergent effects in different phases or contexts of adipocyte differentiation. For example, during early stages of adipocyte differentiation, large doses of atRA act as a powerful inhibitor of this process (7–10), but lower doses of atRA (1 pM to 10 nM range) had a proadipogenic effect (42). Similar proadipogenic effects were demonstrated *in vivo*, where supplementation with atRA rescued the impaired adipogenesis phenotype observed in mice deficient in hormone-sensitive lipase (40). Some gene products shown to have divergent roles during adipocyte differentiation are members of the mitogen-activated protein kinase family. Extracellular signal-regulated kinase-1 (ERK1), for example, is required in the proliferative phase of adipocyte differentiation, as seen in 3T3-L1 cells with suppressed expression of ERK1 (43), or in *Erk1*$^{-/-}$ ES cells and mice that exhibit reduced adipogenic potential (44). In contrast, ERK1 activity leads to phosphorylation of PPARγ, which inhibits differentiation at later stages (45, 46). We propose that products of RetSat might also exert both proadipogenic and antiadipogenic effects on adipose differentiation in a stage-dependent manner. The time frame of RetSat expression suggests that it is predominantly expressed at later stages of differentiation, so it could be involved in the regulation of mature adipose cell function. Consistent with this idea, we observed increased PPARγ signaling and increased adipose tissue formation in the absence of RetSat. These results might suggest that RetSat catalyzes the formation of antagonists of PPARγ, leading to increased PPARγ signaling in the absence of RetSat. What is interesting is that besides activating RARs, DROL can antagonize PPARα but not PPARγ (28). On the basis of the levels observed for DROL *in vivo*, it is unlikely that DROL achieves cellular concentrations sufficient to antagonize PPARα in a physiological setting. But it is possible that other unpredicted/unstudied downstream DROL metabolites could act as PPARγ antagonists *in vivo*.

Our previous studies indicate that RetSat catalyzes the conversion of atROL into (*R*)-DROL (25), which is then converted to (*R*)-DRA (27), a possible agonist of RAR (26–28). Here, we show that RetSat is required for the formation of dihydroretinoids *in vivo*. This important finding demonstrates that *RetSat*$^{-/-}$ mice represent a valuable tool for investigating the physiological role of dihydroretinoids *in vivo*. Results derived from tissue culture models of adipogenesis have led to the suggestion that RetSat could have additional enzymatic activities in adipocytes other than just saturating atROL (30). In these studies, the block in adipocyte differentiation caused by ablation of RetSat expression in 3T3-L1 cells was not rescued by supplementation with the proposed product of RetSat, (*R*)-DROL (30). However, the possibility cannot be excluded that there are other retinoid substrates for RetSat that lead to formation of bioactive retinoids. By using *RetSat*$^{-/-}$ mice, one can assess the physiological significance of other candidate products of RetSat by examining the effects of their supplementation on the formation of adipose stores. Future studies aimed at elucidating the role of RetSat *in vivo* with *RetSat*$^{-/-}$ mice will be necessary to establish the role and significance of dihydroretinoids or other putative products during adipocyte differentiation. FJ

The authors thank members of the K.P. and J.V. laboratories and Dr. Leslie Webster Jr. for critical reading of the manuscript. This research was supported in part by U.S. Public Health Service grants EY01730, EY019478, EY015399, and EY08061 from the National Eye Institute (National Institutes of Health, Bethesda, MD, USA) to K.P., and grants SAF 2007-63880-FEDER and PGIDIT07PXIBIB3174174PR to A.R.D. and R.A.

REFERENCES

1. Chambon, P. (1996) A decade of molecular biology of retinoic acid receptors. *FASEB J.* **10,** 940–954
2. Giguere, V., Ong, E. S., Segui, P., and Evans, R. M. (1987) Identification of a receptor for the morphogen retinoic acid. *Nature* **330,** 624–629
3. Petkovich, M., Brand, N. J., Krust, A., and Chambon, P. (1987) A human retinoic acid receptor which belongs to the family of nuclear receptors. *Nature* **330,** 444–450
4. Ross, S. A., McCaffery, P. J., Drager, U. C., and De Luca, L. M. (2000) Retinoids in embryonal development. *Physiol. Rev.* **80,** 1021–1054
5. Bonet, M. L., Ribot, J., Felipe, F., and Palou, A. (2003) Vitamin A and the regulation of fat reserves. *Cell. Mol. Life Sciences* **60,** 1311–1321
6. Ziouzenkova, O., and Plutzky, J. (2008) Retinoid metabolism and nuclear receptor responses: New insights into coordinated regulation of the PPAR-RXR complex. *FEBS Lett.* **582,** 32–38
7. Murray, T., and Russell, T. R. (1980) Inhibition of adipose conversion in 3T3–L2 cells by retinoic acid. *J. Supramol. Struct.* **14,** 255–266
8. Kuriharcuch, W. (1982) Differentiation of 3t3–F442a cells into adipocytes is inhibited by retinoic acid. *Differentiation* **23,** 164–169
9. Schwarz, E. J., Reginato, M. J., Shao, D., Krakow, S. L., and Lazar, M. A. (1997) Retinoic acid blocks adipogenesis by inhibiting C/EBPβ-mediated transcription. *Mol. Cell. Biol.* **17,** 1552–1561
10. Xue, J. C., Schwarz, E. J., Chawla, A., and Lazar, M. A. (1996) Distinct stages in adipogenesis revealed by retinoid inhibition of differentiation after induction of PPAR gamma. *Mol. Cell. Biol.* **16,** 1567–1575
11. Mercader, J., Ribot, J., Murano, I., Felipe, F., Cinti, S., Bonet, M. L., and Palou, A. (2006) Remodeling of white adipose tissue after retinoic acid administration in mice. *Endocrinology* **147,** 5325–5332
12. Mercader, J., Madsen, L., Felipe, F., Palou, A., Kristiansen, K., and Bonet, M. L. (2007) All-trans retinoic acid increases oxidative metabolism in mature adipocytes. *Cell. Physiol. Biochem.* **20,** 1061–1072

13. Felipe, F., Mercader, J., Ribot, J., Palou, A., and Bonet, M. L. (2005) Effects of retinoic acid administration and dietary vitamin A supplementation on leptin expression in mice: lack of correlation with changes of adipose tissue mass and food intake. *Biochim. Biophys. Acta* **1740,** 258–265
14. Hollung, K., Rise, C. P., Drevon, C. A., and Reseland, J. E. (2004) Tissue-specific regulation of leptin expression and secretion by all-trans retinoic acid. *J. Cell. Biochem.* **92,** 307–315
15. Shin, D. J., and McGrane, M. M. (1997) Vitamin A regulates genes involved in hepatic gluconeogenesis in mice: phosphoenolpyruvate carboxykinase, fructose-1,6-bisphosphatase and 6-phosphofructo-2-kinase/fructose-2,6-bisphosphatase. *J. Nutr.* **127,** 1274–1278
16. Ziouzenkova, O., Orasanu, G., Sharlach, M., Akiyama, T. E., Berger, J. P., Viereck, J., Hamilton, J. A., Tang, G., Dolnikowski, G. G., Vogel, S., Duester, G., and Plutzky, J. (2007) Retinaldehyde represses adipogenesis and diet-induced obesity. *Nat. Med.* **13,** 695–702
17. Jeyakumar, S. M., Vajreswari, A., and Giridharan, N. V. (2006) Chronic dietary vitamin A supplementation regulates obesity in an obese mutant WNIN/Ob rat model. *Obesity* **14,** 52–59
18. Jeyakumar, S. M., Vajreswari, A., and Giridharan, N. V. (2008) Vitamin A regulates obesity in WNIN/Ob obese rat; independent of stearoyl-CoA desaturase-1. *Biochem. Biophys. Res. Commun.* **370,** 243–247
19. Amengual, J., Ribot, J., Bonet, M. L., and Palou, A. (2008) Retinoic acid treatment increases lipid oxidation capacity in skeletal muscle of mice. *Obesity* **16,** 585–591
20. Berry, D. C., and Noy, N. (2009) All-trans-retinoic acid represses obesity and insulin resistance by activating both peroxisome proliferation-activated receptor β/δ and retinoic acid receptor. *Mol. Cell. Biol.* **29,** 3286–3296
21. Anghel, S. I., Bedu, E., Vivier, C. D., Descombes, P., Desvergne, B., and Wahli, W. (2007) Adipose tissue integrity as a prerequisite for systemic energy balance: a critical role for peroxisome proliferator-activated receptor gamma. *J. Biol. Chem.* **282,** 29946–29957
22. Trujillo, M. E., and Scherer, P. E. (2006) Adipose tissue-derived factors: impact on health and disease. *Endocr. Rev.* **27,** 762–778
23. Tsutsumi, C., Okuno, M., Tannous, L., Piantedosi, R., Allan, M., Goodman, D. S., and Blaner, W. S. (1992) Retinoids and retinoid-binding protein expression in rat adipocytes. *J. Biol. Chem.* **267,** 1805–1810
24. Moise, A. R., Isken, A., Dominguez, M., de Lera, A. R., von Lintig, J., and Palczewski, K. (2007) Specificity of zebrafish retinol saturase: formation of all-trans-13,14-dihydroretinol and all-trans-7,8- dihydroretinol. *Biochemistry* **46,** 1811–1820
25. Moise, A. R., Kuksa, V., Imanishi, Y., and Palczewski, K. (2004) Identification of all-trans-retinol:all-trans-13,14-dihydroretinol saturase. *J. Biol. Chem.* **279,** 50230–50242
26. Moise, A. R., Dominguez, M., Alvarez, S., Alvarez, R., Schupp, M., Cristancho, A. G., Kiser, P. D., de Lera, A. R., Lazar, M. A., and Palczewski, K. (2008) Stereospecificity of retinol saturase: absolute configuration, synthesis, and biological evaluation of dihydroretinoids. *J. Am. Chem. Soc.* **130,** 1154–1155
27. Moise, A. R., Kuksa, V., Blaner, W. S., Baehr, W., and Palczewski, K. (2005) Metabolism and transactivation activity of 13,14-dihydroretinoic acid. *J. Biol. Chem.* **280,** 27815–27825
28. Moise, A. R., Alvarez, S., Dominguez, M., Alvarez, R., Golczak, M., Lobo, G. P., von Lintig, J., de Lera, A. R., and Palczewski, K. (2009) Activation of retinoic acid receptors by dihydroretinoids. [E-pub ahead of print] *Mol. Pharmacol.* doi: 10.1124/mol.109.060038
29. Rosen, E. D., Sarraf, P., Troy, A. E., Bradwin, G., Moore, K., Milstone, D. S., Spiegelman, B. M., and Mortensen, R. M. (1999) PPARγ is required for the differentiation of adipose tissue in vivo and in vitro. *Mol. Cell.* **4,** 611–617
30. Schupp, M., Lefterova, M. I., Janke, J., Leitner, K., Cristancho, A. G., Mullican, S. E., Qatanani, M., Szwergold, N., Steger, D. J., Curtin, J. C., Kim, R. J., Suh, M. J., Albert, M. R., Engeli, S., Gudas, L. J., and Lazar, M. A. (2009) Retinol saturase promotes adipogenesis and is downregulated in obesity. *Proc. Natl. Acad. Sci. U. S. A.* **106,** 1105–1110
31. Lopez, I. P., Milagro, F. I., Marti, A., Moreno-Aliaga, M. J., Martinez, J. A., and De Miguel, C. (2004) Gene expression changes in rat white adipose tissue after a high-fat diet determined by differential display. *Biochem. Biophys. Res. Commun.* **318,** 234–239
32. Lopez, I. P., Milagro, F. I., Marti, A., Moreno-Aliaga, M. J., Martinez, J. A., and De Miguel, C. (2005) High-fat feeding period affects gene expression in rat white adipose tissue. *Mol. Cell. Biochem.* **275,** 109–115
33. Lillie, R. D., and Fullmer, H. M. (1976) *Histopathologic Technique and Practical Histochemistry*, McGraw-Hill, New York
34. Yu, H., Shimakawa, A., McKenzie, C. A., Brodsky, E., Brittain, J. H., and Reeder, S. B. (2008) Multiecho water-fat separation and simultaneous R2* estimation with multifrequency fat spectrum modeling. *Magn. Reson. Med.* **60,** 1122–1134
35. Johnson, D. H., Flask, C. A., Ernsberger, P. R., Wong, W. C., and Wilson, D. L. (2008) Reproducible MRI measurement of adipose tissue volumes in genetic and dietary rodent obesity models. *J. Magn. Reson. Imaging* **28,** 915–927
36. Kane, M. A., Chen, N., Sparks, S., and Napoli, J. L. (2005) Quantification of endogenous retinoic acid in limited biological samples by LC/MS/MS. *Biochem. J.* **388,** 363–369
37. Kane, M. A., Folias, A. E., Wang, C., and Napoli, J. L. (2008) Quantitative profiling of endogenous retinoic acid in vivo and in vitro by tandem mass spectrometry. *Anal. Chem.* **80,** 1702–1708
38. Ribot, J., Felipe, F., Bonet, M. L., and Palou, A. (2001) Changes of adiposity in response to vitamin A status correlate with changes of PPARγ 2 expression. *Obes. Res.* **9,** 500–509
39. Zhang, M., Hu, P., Krois, C. R., Kane, M. A., and Napoli, J. L. (2007) Altered vitamin A homeostasis and increased size and adiposity in the rdh1-null mouse. *FASEB. J.* **21,** 2886–2896
40. Strom, K., Gundersen, T. E., Hansson, O., Lucas, S., Fernandez, C., Blomhoff, R., and Holm, C. (2009) Hormone-sensitive lipase (HSL) is also a retinyl ester hydrolase: evidence from mice lacking HSL. *FASEB J.* **23,** 2307–2316
41. Hessel, S., Eichinger, A., Isken, A., Amengual, J., Hunzelmann, S., Hoeller, U., Elste, V., Hunziker, W., Goralczyk, R., Oberhauser, V., von Lintig, J., and Wyss, A. (2007) CMO1 deficiency abolishes vitamin A production from beta-carotene and alters lipid metabolism in mice. *J. Biol. Chem.* **282,** 33553–33561
42. Safonova, I., Darimont, C., Amri, E. Z., Grimaldi, P., Ailhaud, G., Reichert, U., and Shroot, B. (1994) Retinoids are positive effectors of adipose cell differentiation. *Mol. Cell. Endocrinol.* **104,** 201–211
43. Sale, E. M., Atkinson, P. G., and Sale, G. J. (1995) Requirement of MAP kinase for differentiation of fibroblasts to adipocytes, for insulin activation of p90 S6 kinase and for insulin or serum stimulation of DNA synthesis. *EMBO J.* **14,** 674–684
44. Bost, F., Aouadi, M., Caron, L., Even, P., Belmonte, N., Prot, M., Dani, C., Hofman, P., Pages, G., Pouyssegur, J., Le Marchand-Brustel, Y., and Binetruy, B. (2005) The extracellular signal-regulated kinase isoform ERK1 is specifically required for in vitro and in vivo adipogenesis. *Diabetes* **54,** 402–411
45. Camp, H. S., and Tafuri, S. R. (1997) Regulation of peroxisome proliferator-activated receptor gamma activity by mitogen-activated protein kinase. *J. Biol. Chem.* **272,** 10811–10816
46. Hu, E., Kim, J. B., Sarraf, P., and Spiegelman, B. M. (1996) Inhibition of adipogenesis through MAP kinase-mediated phosphorylation of PPARgamma. *Science* **274,** 2100–2103

Received for publication September 28, 2009.
Accepted for publication November 5, 2009.